



High-Frequency Nonlinear Doppler Contrast-Enhanced Ultrasound Imaging of Blood Flow

Matthew Bruce^{ID}, Alex Hannah, Ryan Hammond, Zin Z. Khaing, Charles Tremblay-Darveau^{ID}, Peter N. Burns, and Christoph P. Hofstetter

Abstract—Current methods for *in vivo* microvascular imaging (<1 mm) are limited by the tradeoffs between the depth of penetration, resolution, and acquisition time. Ultrasound Doppler approaches combined at elevated frequencies (>7.5 MHz) are able to visualize smaller vasculature and, however, are still limited in the segmentation of lower velocity blood flow from moving tissue. Contrast-enhanced ultrasound (CEUS) has been successful in visualizing changes in microvascular flow at conventional diagnostic ultrasound imaging frequencies (<7.5 MHz). However, conventional CEUS approaches at elevated frequencies have met with limited success, due, in part, to the diminishing microbubble response with frequency. We apply a plane-wave acquisition combined with the non-linear Doppler processing of ultrasound contrast agents at 15 MHz to improve the resolution of microvascular blood flow while compensating for reduced microbubble response. This plane-wave Doppler approach of imaging ultrasound contrast agents also enables simultaneous detection and separation of blood flow in the microcirculation and higher velocity flow in the larger vasculature. We apply singular value decomposition filtering on the nonlinear Doppler signal to orthogonally separate the more stationary lower velocity flow in the microcirculation and higher velocity flow in the larger vasculature. This orthogonal separation was also utilized to improve time-intensity curve analysis of the microcirculation, by removing higher velocity flow corrupting bolus kinetics. We demonstrate the utility of this imaging approach in a rat spinal cord injury model, requiring submillimeter resolution.

Index Terms—Doppler, microbubbles, ultrasound imaging.

Manuscript received March 9, 2020; accepted April 5, 2020. Date of publication April 8, 2020; date of current version August 27, 2020. This work was supported by the Craig H. Neilsen Foundation, DoD CDMRP Translational Award (W81XWH-18-1-0753), and the Raisbeck Foundation. (Corresponding author: Matthew Bruce.)

Matthew Bruce, Alex Hannah, and Ryan Hammond are with the Center for Industrial, University of Washington, Seattle, WA 98104 USA, and also with the Medical Ultrasound and the Applied Physics Laboratory, University of Washington, Seattle, WA 98105 USA (e-mail: mbruce@uw.edu).

Zin Z. Khaing and Christoph P. Hofstetter are with the Department of Neurosurgery, University of Washington, Seattle, WA 98105 USA.

Charles Tremblay-Darveau is with Philips Medical Systems, Bothell, WA 98021 USA.

Peter N. Burns is with the Department of Medical Biophysics, University of Toronto, Toronto, ON M5G 1L7, Canada.

Digital Object Identifier 10.1109/TUFFC.2020.2986486

I. INTRODUCTION

CURRENT methods for *in vivo* microvascular imaging in small animals are limited by the tradeoffs between the depth of penetration, resolution, and acquisition time. For example, microcomputed tomography images vessels down to $10\ \mu\text{m}$ within the tissue (~ 3 mm) but requires sacrificing the animal [1]. Being noninvasive, MRI requires expensive infrastructure, generates relatively low-resolution images, and is sensitive to motion. Fluorescence imaging has a high spatial resolution ($\sim 50\ \mu\text{m}$) and fast acquisition times (~ 200 ms) but is limited in penetration of 1–3 mm [2]. Optical approaches, such as optical computed tomography and photoacoustics, are also limited to imaging depths of a few millimeters [3]. A robust, economical, easy to use, and high-resolution technique to assess the changes in blood flow at depths of 1–3 cm with submillimeter resolution would impact a broad range of preclinical imaging applications and research, ranging in areas such as oncological, cardiac, vascular, and neurological.

Ultrasound has a number of advantages for preclinical imaging. Its real-time imaging capabilities provide a noninvasive, economical tool to assess structural tissue and blood flow changes in longitudinal studies. Newer Doppler approaches enable the visualization of lower velocity blood flow in smaller vasculature [2]. However, as the Doppler shifts from a lower velocity blood flow approach that of tissue motion, the visualization of blood flow in smaller vasculature, including perfusion in the microcirculation, is lost [3].

Contrast-enhanced ultrasound (CEUS) removes this limitation of detection of lower velocity blood flow based solely on velocity differences by the addition of intravenously injected microbubbles. However, traditional approaches of CEUS requiring higher resolution (\sim submillimeter) have been hampered by the diminishing oscillatory response from microbubbles as the frequency increases (>7 MHz) [4]. Super-resolution approaches borrowed from optical microscopy have been applied to CEUS producing amazing maps of different vascular trees [5]. However, super-resolution approaches currently require long acquisition times (\sim minutes) and are sensitive to motion artifacts. We demonstrate that the plane-wave nonlinear Doppler approaches can both compensate for the weak nonlinear response from microbubbles at elevated frequencies

(15 MHz) through signal averaging while, at the same time, enabling the segmentation of higher velocity blood flow in typical preclinical scenarios (e.g., tissue motion and limited acquisition times) [6], [7]. Fig. 2 shows the difference in resolution currently available with conventional contrast imaging approaches on commercially available diagnostic ultrasound systems at a lower frequency (Epiq, Philips, Bothell, WA, USA) and our 15-MHz perfusion image.

In the previous work, we have demonstrated the ability of amplitude- and phase-modulated Doppler sequences with conventional Doppler processing to separate low-velocity microbubbles in the microcirculation from higher velocity microbubbles in larger vasculature [8]. More recently, we have applied this approach to investigate the blood flow changes in a rodent spinal cord injury model [9]. In this work, we describe the technical details used by Khaing *et al.* [9] and demonstrate the ability to visualize the *in vivo* bolus-kinetics differences in the microcirculation and larger vasculature. Finally, the impact of *in vivo* respiratory motion is demonstrated in a more challenging application of an abdominal mouse model.

II. THEORY

A. Nonlinear Doppler Sequences for Microbubble Imaging

Nonlinear pulsing sequences, where modulation of phase or amplitude is applied to a pulse ensemble, have been developed to separate the larger nonlinear response of microbubble from tissue signals at low-pressure amplitudes ($\sim 50\text{--}100$ kPa), enabling visualization of microbubbles in the microcirculation [6], [10], [11]. Amplitude modulation (AM) was originally designed for diagnostic scanners that could not invert or poorly invert phase and is now commonly used on clinical systems due to its superior tissue echo cancellation and advantages in attenuation [7]. We have previously proposed a signal processing scheme enabling AM Doppler. An amplitude-modulated Doppler vector is acquired by repeatedly insonating the microbubbles with “full” (1) and “half” (1/2) amplitude pulses [7]. With normalization, the linear and nonlinear Doppler components separate to 0 Hz and the Nyquist frequencies, respectively. This enables separate the processing of both the linear and nonlinear Doppler components, as described earlier [8], [12]. However, integrating this approach into a multiangle plane-wave sequence would result in large interpulse time intervals, when combined with motion, resulting in difficulties for the linear cancellation of background tissue. In this article, the pulsing sequence consisted of amplitude-modulated sequence transmitted for each angle of a multiangle plane-wave sequence, generating a nonlinear-Doppler pulse, which was then repeated generating a nonlinear Doppler sequence. Multiangle plane-wave acquisitions enable a way to tradeoff transmit aperture and resulting lateral resolution and off-axis artifacts, with frame rate [2], [13]. The group of both nonlinear pulsing sequences can then be first summed to produce a nonlinear image for each angle, where the angles can then be summed to produce a nonlinear synthetic compound image or the Doppler PRI.

This acquisition sequence is repeated, generating a nonlinear synthetically compounded Doppler sequence.

B. Nonlinear Doppler Processing

Within the nonlinear Doppler sequence, the stronger nonlinear echoes from microbubbles are separated from the weaker tissue echoes, arising from nonlinear sound propagation. Doppler processing can be applied to extract the higher velocity microbubbles from the lower velocity ones in the microcirculation. Here, we utilize the singular value decomposition (SVD) approach for the separation of Doppler velocities. SVD has been shown to be an effective filtering approach to separate higher velocity blood flow from lower velocity tissue motion [14]. This spatiotemporal approach decomposes a region of interest (ROI) or entire image into orthogonal spaces

$$S = U \Sigma V^H \quad (1)$$

whereas described by Demené *et al.* [14], S is the nonlinear Doppler ensemble reshaped in a 2-D space-time form with dimensions $(n_x \times n_z, n_{\text{pri}})$, U ($n_x \times n_z, n_x \times n_z$) is the column space or spatial singular vectors of S , V ($n_{\text{pri}} \times n_{\text{pri}}$) is the row space or temporal singular vectors of S , and Σ ($n_x \times n_z, n_{\text{pri}}$) is the diagonal matrix containing the singular values of S and H that stands for the Hermitian conjugate transpose. As the singular values of Σ are ordered from the largest to the smallest, S can be decomposed as

$$S = \sum_{i=1}^{\text{rank}(S)} \lambda_i U_i V_i^H. \quad (2)$$

The larger singular values capture the spatial areas where the nonlinear Doppler ensemble is more stationary, corresponding to, in our case, lower velocity microbubbles in the microcirculation. Smaller singular values capture spatial areas where microbubbles have less coherence due to higher velocities. As a result, lower and higher velocity signals can be separated

$$S_{\text{perf}} = \sum_{i=1}^{N_{\text{perf}}} \lambda_i U_i V_i^H \quad (3)$$

$$S_{\text{flow}} = \sum_{k=N_{\text{perf}}+1}^{N_{\text{flow}}} \lambda_k U_k V_k^H \quad (4)$$

where S_{perf} and S_{flow} are the perfusion and flow subspaces, respectively, and N_{perf} and N_{flow} are the dimensions of the respective perfusion and flow subspaces. S_{perf} and S_{flow} ($n_x \times n_z, n_{\text{pri}}$) can then be reshaped for image display of the Doppler estimates to image dimensions (n_x, n_z, n_{pri}). Estimates for each signal can now be obtained. Fig. 1 illustrates this segmentation and the distribution of singular values and flow components. To display the perfusion image, we use the magnitude of the first lag of the biased autocorrelation $R(1)$ for its advantage in noise over the traditional power $R(0)$ [15]. In comparison to the traditional display of a single nonlinear image, the perfusion signal benefits in SNR gained over the ensemble compared with a single nonlinear Doppler image in addition to the removal of the higher velocity

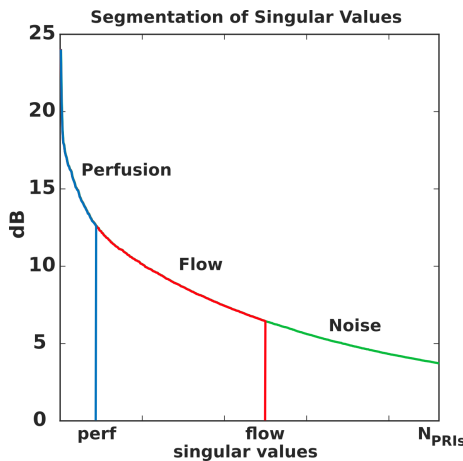


Fig. 1. Illustration of the segmentation of singular values to separate lower velocity microbubble flow in the microcirculation, higher velocity flow in the larger vasculature, and noise. N_{PRIs} : number of nonlinear Doppler pulses or pulse repetition intervals.

flow signal. To display the flow image, again the first lag of the autocorrelation, $R(0)$, is used to display the “power” of the flow image. The phase of $R(1)$ can then be used to estimate velocity [16].

One of the practical challenges in signal decomposition approaches (e.g., Fourier, wavelet, eigen, or singular vector) is in the selection of the signal subspaces. In this work, the selection of the two subspaces for low-velocity microbubble flow in the smaller vasculature and higher velocity flow in the larger vasculature was driven by smoothness or reduction in speckle variance associated with increasing the dimension of the perfusion subspace. As more singular vectors are included in the perfusion subspace (i.e., increasing $\text{dim}(S_{\text{perf}})$), the speckle variance is reduced due to differences in the alignment of speckle between perfusion subvectors or blurring of the speckle [17]. The rational was to increase $\text{dim}(S_{\text{perf}})$ to the point that the larger vessels are clearly visualized and free from spatially distributed lower velocity signals. $\text{SNR}_{\text{speckle}}$ of S_{perf} as defined by

$$\text{SNR}_{\text{speckle}} = \mu/\sigma \quad (5)$$

where μ and σ are the mean and standard variation of a region containing at least three cells of speckle were followed until reaching a threshold to determine $\text{dim}(S_{\text{perf}})$.

III. METHOD

A. Acquisition Sequences for Microbubble Imaging

The Vantage ultrasound research platform (Verasonics, Kirkland, WA, USA) was used to program multiangle plane-wave nonlinear Doppler sequences, using a 15-MHz linear array transducer (Vermon, Tours, France). The 15-MHz two-cycle plane-waves were emitted using the full linear array aperture, and the resulting echoes were recorded from every transducer element. The multiangle plane-wave nonlinear Doppler sequence was previously described, where amplitude modulated pulses are transmitted for each angle [8]. On reception for each angle after bandpass filtering at 15 MHz

and sampled at 62.5 MHz, the amplitude modulated pulses are scaled and summed producing a nonlinear angled image, which is then delay-and-sum beamformed. The angles of the plane-wave sequence are then coherently combined producing a synthetic nonlinear Doppler image. This sequence of multi-angle amplitude-modulated plane waves is then repeated by the ensemble length. The abovementioned SVD decompositions were then performed in separating lower and higher velocity flow.

B. In Vitro Experiment

The *in vitro* experimental setup consisted of a 2-mm-diameter dialysis tube mounted in an acrylic box filled with distilled water. The transducer was positioned above the tube with a locking articulated arm (FISSO, Switzerland). An infusion pump (Chemex N3000, Stafford, TX, USA) with a 50-mL syringe was used to push a constant flow of 0.05 mL of Definity diluted in 200-mL distilled water through the dialysis tube. Using the Vantage ultrasound system, the acquisition consisted of a 0° angle plane-wave nonlinear Doppler sequence at a 5-kHz PRF, with the processing described earlier. Peak velocity of 3 cm/s was measured using PW Doppler with the Epiq diagnostic ultrasound system (Philips Ultrasound, Bothell, WA, USA) for validation.

C. In Vivo Experiments

Surgical procedures were performed according to approved IACUC protocol following all appropriate guidelines from the University’s Animal Welfare Assurance (A3464-01) as well as the NIH Office of Laboratory Animal Welfare (OLAW). Female Sprague Dawley (Harlan Labs, Indianapolis, IN, USA) rats weighing 250 g at the time of experiment were used. The rats were anesthetized using isoflurane (5% to induce and 2.5%–3% to maintain general anesthesia), and the area overlying the T7/T8 vertebrae was shaved, cleaned, and sterilized. A longitudinal incision was carried out overlying the T6–T11 area using a #10 scalpel blade. After subperiosteal dissection of paraspinal muscles, a laminectomy was performed to expose the spinal cord from T6 to T10. A contusion-type lesion was produced using the Infinite Horizon (IH) Impactor device (Precision Systems & Instrumentation, Lexington, KY, USA). The rodent received a 150-kDyn (impact force) spinal cord contusion using the IH impactor device at the T10 level. This injury force results in a moderate contusion injury in female rats in this weight range. Animals received lactated Ringers solution during anesthesia (subcutaneous; 5 mL for every 2 h).

Following laminectomy, the ultrasound probe was positioned 5 mm from the spinal cord and over the center sagittal plane. Ultrasound gel between the cord and probe positioned longitudinally relative to the spinal cord slice while leaving free access to the posterior part of the cord. For each contrast injection, a bolus of 0.1 mL of Definity (Lantheus, NJ, USA) was injected intravenously followed by a 0.2-mL saline flush. The 600 nonlinear Doppler ensembles were acquired at a 10-kHz PRF with a mechanical index of 0.04 before

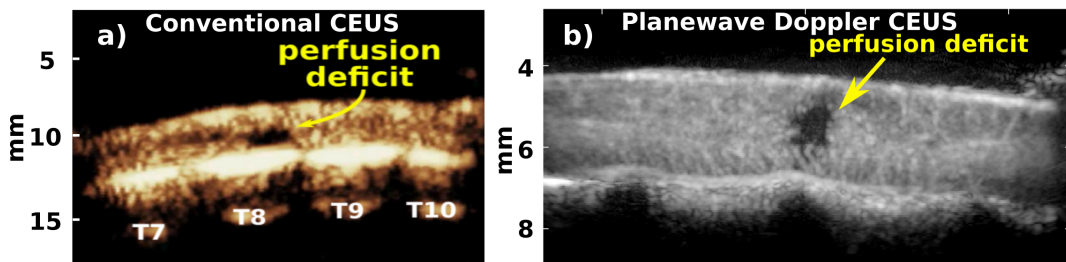


Fig. 2. Comparison of perfusion deficit postinjury with (a) EPIQ L12-3 CEUS and (b) plane-wave Doppler CEUS showing marked improvement dynamic range and resolution.

and immediately following injury. This choice of acquisition length and PRF enabled the capture of several cardiac cycles and spectral content of blood flow in the rat spinal cord. For comparison of perfusion images, an L12-5 transducer in contrast mode using the Epiq diagnostic ultrasound system (Philips, USA) was used to acquire images following injury. In addition, the second acquisition of 40 nonlinear Doppler ensembles was also acquired at 16 Hz for 30 s in order to follow the passage of the bolus injection following injury. The bolus kinetics of different regions of an injured spinal cord followed and compared for the two different flow components. The mean power of the ROIs was calculated for each acquisition capturing the passage of the bolus through the different vasculatures.

The use of the rat spinal cord injury model enables us to demonstrate the ability to detect a change in blood flow in both the larger and smaller vasculature. In addition, the amount of cardiac and respiratory motion, although more than the brain, is much less than imaging in the abdomen.

IV. RESULTS

As mentioned in Section I, Fig. 2 shows the difference in resolution currently available with conventional contrast imaging approaches on commercially available diagnostic ultrasound systems at lower frequencies (~ 5 MHz) and our approach at 15 MHz.

A. In Vitro Results of Flow Perfusion Segmentation

Fig. 3 illustrates the ability of SVD processing of the nonlinear Doppler acquisition to segment stationary microbubbles in the presence of flowing microbubbles. Fig. 3(a) and (b) shows the stationary microbubble signal projected onto the first singular vector. In Fig. 3(b), the stationary microbubbles adherent primarily to the top vessel wall due to buoyancy are separated from the surrounding flowing microbubbles shown in Fig. 3(d). In Fig. 3(c), no signal is projected on to the flow subspace due to the absence of flowing microbubbles.

B. In Vivo Results of Flow and Perfusion Segmentation

Fig. 4 contrasts the difference between the linear and nonlinear Doppler signals. While both Doppler signals provide macrovascular flow, the nonlinear Doppler signal's low-velocity components are free from tissue signal enabling

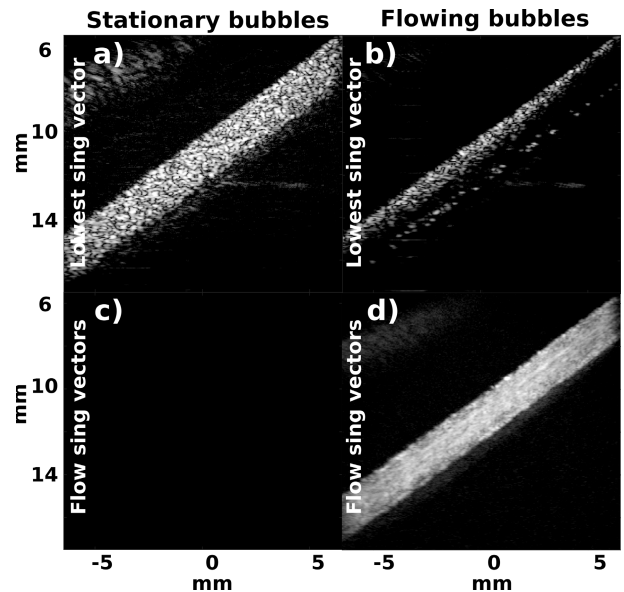


Fig. 3. Illustration of the separation of stationary and flowing microbubbles by SVD processing with 20 dB of dynamic range. (a) Stationary microbubble signal captured by the first singular vectors. (b) Stationary microbubbles when microbubbles are flowing through the tube, where floating microbubbles can be seen accumulating on the top wall. (c) Removal of stationary signal by use of flow singular vectors. (d) Moving microbubble signals projected onto flow subspace.

visualization of microbubbles and blood flow in the microcirculation [see Fig. 4(a)], while the linear Doppler signal's low-velocity components show a combination both microbubble signal and tissue [see Fig. 4(b)]. Both Doppler signals segment macrovascular flow, as shown in Fig. 4(c) and (d). However, the linear macrovascular flow [see Fig. 4(d)] has an advantage of roughly 15 dB over the nonlinear flow in Fig. 4(c).

Fig. 5(a) and (b) illustrates the *in vivo* segmentation of low-velocity blood flow (\sim mm/s) and higher velocity blood flow (>0.5 cm/s) before and immediately after injury. Fig. 5(a) and (b) shows the power of the segmented lower velocity flow and a deficit of flow at the site of contusion injury [see Fig. 5(b)]. Fig. 5(c) and (d) shows the higher velocity flow in the larger vasculature, also with a deficit of vasculature at the site of contusion. Fig. 6 illustrates the increase in SNR as N_{perf} [i.e., $\dim(S_{\text{perf}})$] is increased and the resulting smoothing of speckle in the perfusion image of Fig. 5(a) and (b). To separate low and high velocity flows, the flattening of the SNR, as shown in Fig. 6, provided an empirical guide for

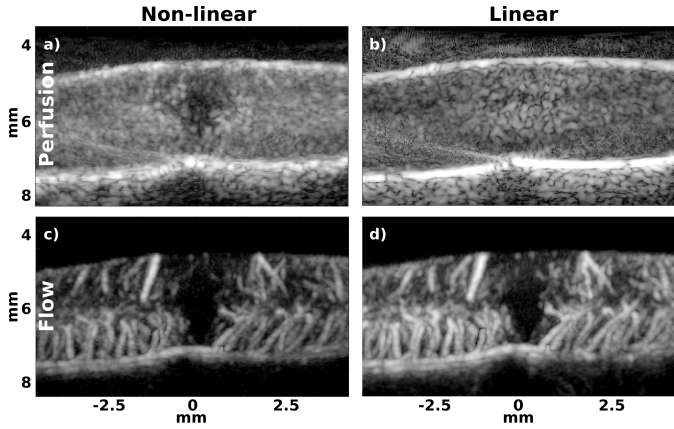


Fig. 4. Illustration of the linear and nonlinear Doppler microbubble signals of a vascular deficit in contused tissue of a rat spinal cord injury model. (a) Stationary component of the nonlinear Doppler signal from microbubbles showing loss of flow in the microcirculation. (b) Stationary component of the mix of tissue and microbubble linear Doppler signals. (c) and (d) Vascular flow images of the nonlinear and linear Doppler signals, respectively. The dynamic ranges of (a)–(d) are 35 and 40 dB, respectively.

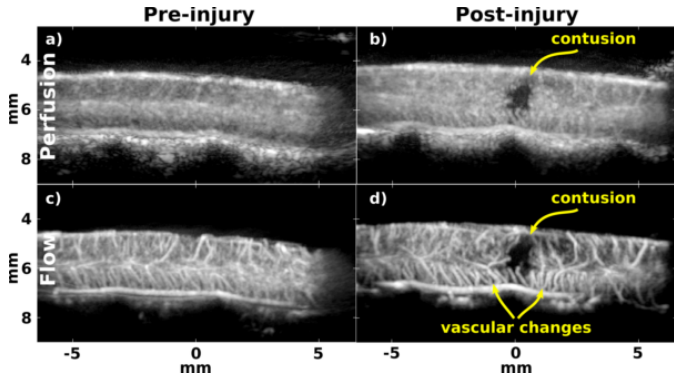


Fig. 5. Separation of perfusion and flow in preinjury and postinjury in rat spinal cord resting on top of vertebral bones. (a) and (b) Lower velocity flow following SVD segmentation with a deficit of flow in the contused region in (b). (c) and (d) Higher velocity flow following SVD segmentation where the post injury image shows a lack of flow in larger vasculature in the contused region and dorsal vascular alterations. Perfusion and flow images have 35 and 25 dB of dynamic range, respectively.

the selection of the threshold N_{perf} . A value of 50 in this case enabled the higher velocity flow projection to be contamination free of spatially distributed lower velocity flow.

C. Time Intensity Curves of Bolus Injection

Fig. 7 illustrates the sequence of shorter ensemble lengths capturing the passage of a bolus through injured contused spinal cord tissue. Fig. 7(a) illustrates the differences in washin and washout kinetics for larger vasculature for the different ROIs shown in Fig. 7(f). Fig. 7(b) shows differences in washin and washout kinetics for microbubble passage through the microcirculation for the different ROIs shown in Fig. 7(c). A 1-s difference can be seen between the arrival of microbubbles in the larger vasculature and microbubbles arriving in the microcirculation. A 1-s difference is also observed in the arrival of microbubbles in the microcirculation of the medulla

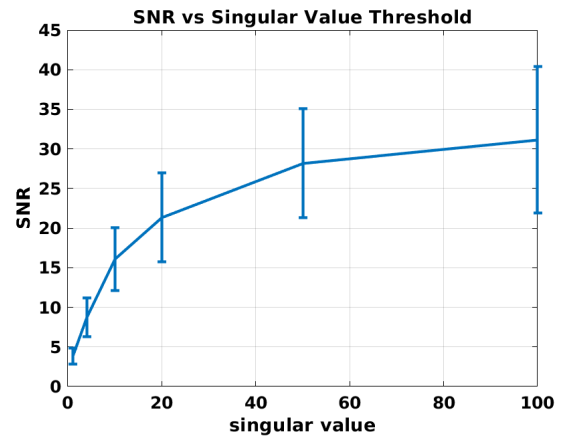


Fig. 6. Illustration of the change in SNR or smoothing of the speckle used to estimate a threshold in the segmentation between perfusion and flow of a 1 mm \times 1 mm region in the center of spinal cord of Fig. 5(b).

(ROI_{pink}) and adjacent tissue to the injury site (ROI_{green}). Varying delays in the arrival of microbubbles can be seen in the dorsal aspects of the spinal cord. Fig. 7(c) and (d) shows the differences in washin of the microcirculation at three different time points. Fig. 7(e)–(h) shows the differences in washin of the larger vasculature. As seen earlier in Fig. 5, a complete loss of signal is observed in both the perfusion and larger vasculature images.

V. DISCUSSION

Current methods (e.g., optical approaches, microCT, and MR) for *in vivo* microvascular imaging tradeoff compromise in the depth of penetration, resolution, acquisition time, and radiation dose. Nonlinear plane-wave imaging of microbubbles offers a way to compensate for the diminishing microbubble response with the increasing frequency needed to image smaller vasculature [4], [18], [19]. In addition, the high frame rate of a plane-wave approach enables Doppler processing over the entirety of the image [20]. Combining nonlinear pulsing sequences with plane-wave acquisitions, we have demonstrated that the nonlinear Doppler CEUS enables visualization and separation of blood flow changes in both the microcirculation and macrocirculation, not previously shown at an elevated frequency of 15 MHz. The details of the effects of the AM within a Doppler acquisition on the linear and nonlinear Doppler components are described in [8]. Conventional nonlinear imaging of microbubbles provides the visualization of blood flow where the flow in the microcirculation and larger vasculature are mixed together. Visualization of the arterial vasculature can be observed at the beginning of a bolus but is obscured after the filling of the microcirculation. This nonlinear Doppler approach inherently has access to both parts of the vascular tree.

The ability of SVD decomposition of a plane-wave nonlinear Doppler sequence to separate stationary from higher velocity microbubbles was demonstrated in a controlled *in vitro* setup. Two different acquisition sequences were utilized for the evaluation of *in vivo* imaging with this approach. The first acquisition sequence consisted of a continuous nonlinear

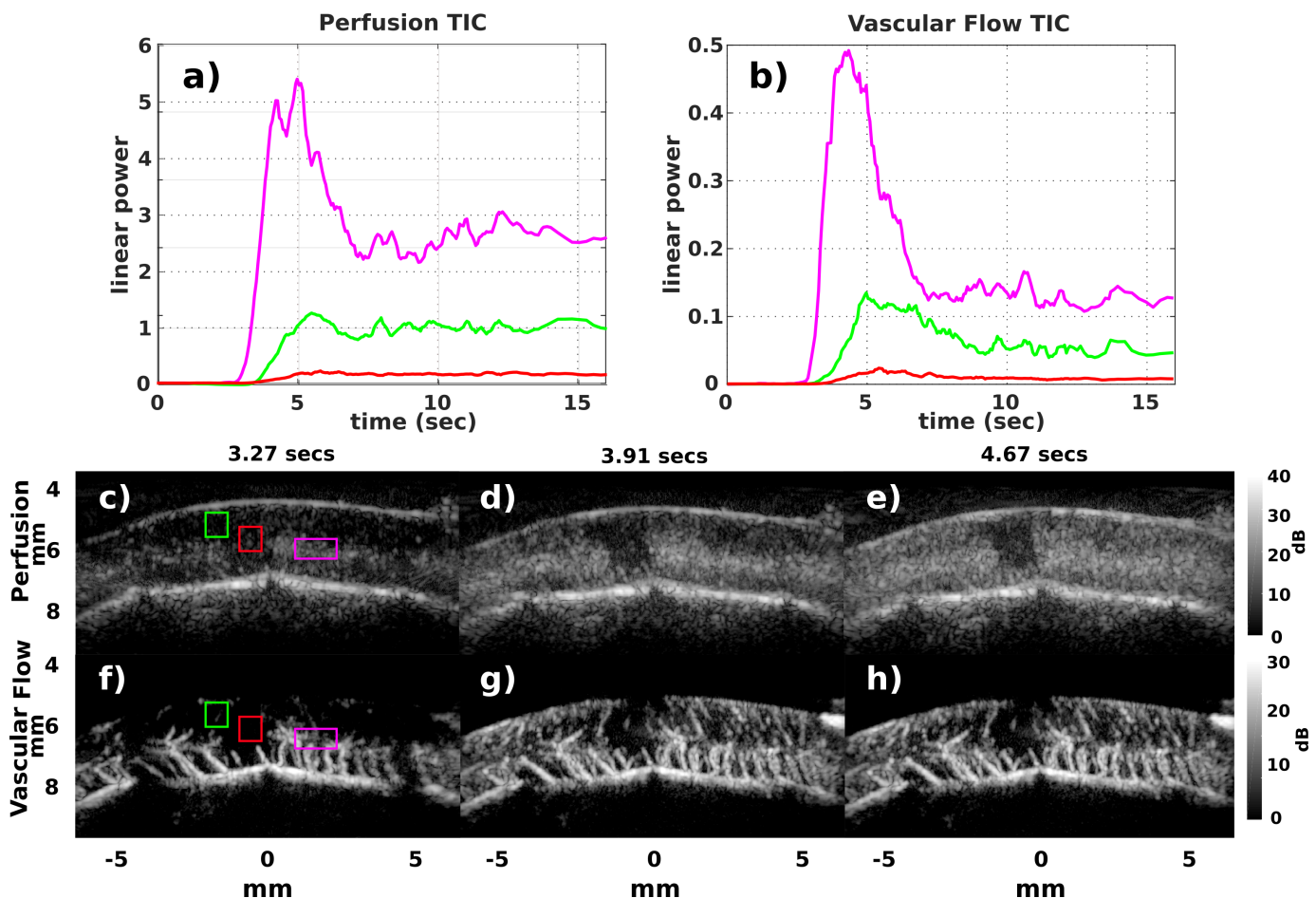


Fig. 7. Illustration of differences in the passage of a microbubble bolus through an ROI in the medulla, adjacent and at the site of injury. (a) Washin and washout of microbubbles in the microcirculation for the regions of 1c. (b) Washin and washout of microbubbles in the larger vasculature for three different regions illustrated in 1f. (c)–(e) Images of three time points of the arrival of microbubbles in the microcirculation. (f)–(h) Images of three time points of the arrival of microbubbles in the larger feeding vasculature.

Doppler sequence just over 1 s. With plane-wave acquisitions, the fine temporal sampling over this time enabled both a benefit in SNR for the perfusion signal and large dimensions for both the flow and perfusion subspaces. Although not shown here, the spectral content of the flow subspace enables the visualization of the velocity distribution in the larger vasculature over the image. Many approaches are possible for the thresholding of the perfusion and vascular flow subspaces of the SVD decomposition [21]. We found thresholding the perfusion and flow subspaces by the increase in SNR or smoothing of the perfusion speckle to provide a reasonable border in subspaces, enabling the capture of the lower velocity vasculature in the subspace without too much contamination of the more spatially distributed perfusion subspace.

The second acquisition sequence consisted of shorter nonlinear Doppler sequences acquired at 16 Hz to capture the passage of bolus through injured contused spinal cord tissue. Differences in the spatial distribution and arrival times of microbubbles in both the microcirculation and larger vasculature were observed surrounding the contusion injury. In addition, the segmentation of both perfusion and vascular flow enabled visualization of the delay between the arrival time in the vasculature and, finally, in the microcirculation not previously observed.

In vivo results were demonstrated on a rodent spinal cord injury model, where this approach is being utilized to explore the changes in blood flow associated with spinal cord contusions [9]. In this work, we observed hypoechoic regions of both the S_{perf} and S_{flow} subspaces of contused tissue with disrupted vasculature, which resolved outside the injury site (see Fig. 5). In terms of bolus kinetics, we observed delays in the arrival time of microbubbles in both of these subspaces in dorsal regions extending both rostrally and caudally. In addition, morphological changes were observed in ventral vasculature, where rostral vessels were pushed down (i.e., closer to horizontal) and dorsal vasculature was pushed up (i.e., closer to vertical) with some additional tortuosity changes [see Fig. 5(d)]. Tortuous vessels arise in numerous organs and scenarios. Notably, one of these situations is in hypertension, where tortuous vessels have been observed in coronary, cerebral, and retinal arteries [22].

A. Comparison of Nonlinear Doppler and Super-Resolution Approaches

Recently, super-resolution approaches have demonstrated remarkable results and growing research interest [23]. However, the majority of these approaches utilize the linear

component of microbubble responses. An advantage in terms of signal-to-noise of this approach is in leveraging the entirety of the temporal microbubble response available within the limited bandwidth of the transducer. However, as the linear microbubble response is mixed in with backscatter from surrounding tissue and also of similar amplitude [see Fig. 4(b)], a corresponding disadvantage is the need to separate the microbubble response from background tissue to perform microbubble tracking. This separation has relied on velocity differences between the microbubbles in the vasculature and surrounding tissue and temporal filtering, limiting the detection and tracking of lower velocity microbubbles in smaller vasculature. This limitation is the same experienced in the Doppler approaches to visualize low-velocity blood flow in smaller vasculature and microcirculation without microbubbles.

A distinction in the approach presented here is the use of the nonlinear component of microbubble responses to separate microbubble from background tissue, enabling visualization of microbubbles in the entire vascular tree not possible with traditional super-resolution approaches. The advantage being the separation of microbubble and tissue is independent of velocity, with the ability to segment both stationary and low-velocity microbubbles in the microcirculation (mm/s) [see Fig. 4(a)]. This advantage comes at the price of relying on the weaker nonlinear microbubble response, especially at elevated frequencies (>7.5 MHz). The advantages and disadvantages of the linear and nonlinear microbubble signals to visualize blood flow are explored in [12].

Both plane-wave nonlinear Doppler and super-resolution approaches trade off temporal resolution and resulting motion artifacts for the visualization and quantification of blood flow with microbubbles, beyond the capability of nonenhanced Doppler. The nonlinear Doppler advantages consist of shorter acquisition times (millisecond to seconds) and the ability to tradeoff integration time (i.e., ensemble length) with frame rate for improvements in SNR and detecting low-velocity blood flow in smaller vasculature. Super-resolution approaches offer marked advantages in resolution with the tradeoff in acquisition/integration time on the order of minutes to 10's of minutes. A key difference being super-resolution approaches rely on lower concentrations of microbubbles to isolate singular scatters for tracking and, thus, longer acquisition times for microbubbles to traverse the branches of the vascular tree. At the same time, considerable efforts are being applied toward reducing the acquisition time of super-resolution approaches by permitting higher concentrations. Approaches that exploit sparsity or deep learning to facilitate the separation and tracking of super-resolution of overlapping microbubble signals are some examples of this research [24]–[26].

Although in-plane motion can be compensated by preregistration or alignment of frames, out-of-plane motion remains a challenge with 1-D arrays, which, in many practical scenarios, can be difficult, where respiratory- or cardiac-induced motion is combined with limited acoustic access. For example, Fig. 8 shows the effect of respiratory motion and temporal blurring in a mouse, where respiration rates can vary 1–3 Hz. Another extreme example of limited temporal windows due to high-velocity tissue motion would be cardiac imaging of

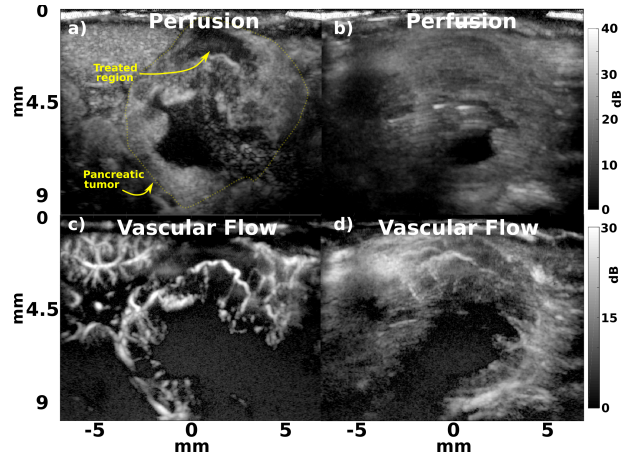


Fig. 8. Pancreatic lesion in a mouse illustrating the effect of respiratory motion. (a) Perfusion image of showing a large cystic region, within a stationary portion of the respiratory cycle. (b) Perfusion image using an acquisition with a temporal over the entirety of the respiratory cycle (~ 1 Hz) showing the resulting blurring. (c) Vascular flow image within a stationary portion of the respiratory cycle. (d) Vascular flow image illustrating the resulting blurring as described in (b).

rodents, where heart rates are on the order of hundreds of beats per minute.

The nonlinear Doppler approach here utilizes high concentrations of microbubbles where there are enough microbubbles in the microcirculation to develop speckle patterns, which develops with multiple microbubbles within the point spread function. The consequence of imaging tissue with the vasculature populated with several microbubbles per sample volume is the ability to image the blood flow dynamics of the entire vascular tree with real-time frame rates (>16 Hz). In contrast, the temporal tradeoff super-resolution approaches use to achieve subdiffraction limited spatial resolutions that make them an attractive approach, where tissue motion is limited or can be controlled or corrected for.

B. Limitations

Limitations of this technique include challenges of dealing with off-axis scatterers associated with plane-wave acquisitions. In this case, the vertebral bones can cause significant off-axis issues, as shown in Fig. 5(a) and (c), for the perfusion images depending on the angle of the transducer with the vertebral bones. Most of these artifacts are removed from the flow images due to the SVD wall filter.

VI. CONCLUSION

It was found that SVD applied to a nonlinear Doppler sequence could be used both to improve the SNR and dynamic range of perfusion signals while, at the same time, enabling visualization and quantification of higher velocity flow in larger vasculature. This approach was used to observe changes in blood flow associated with spinal cord injury in a rat model but could be broadly applied to the imaging of blood flow in rodents.

ACKNOWLEDGMENT

The authors thank Thanasis Loupas, Yak-Nam Wang, and Tanya Khoklova for illuminating discussions and support given.

REFERENCES

- [1] Y. Cao *et al.*, "Three-dimensional imaging of microvasculature in the rat spinal cord following injury," *Sci. Rep.*, vol. 5, no. 1, p. 12643, Oct. 2015.
- [2] G. Montaldo, E. Mace, I. Cohen, J. Berckoff, M. Tanter, and M. Fink, "Ultrafast compound Doppler imaging: A new approach of Doppler flow analysis," in *Proc. IEEE Int. Symp. Biomed. Imag., Nano Macro*, Apr. 2010, pp. 324–327.
- [3] A. Heimdal and H. Torp, "Ultrasound Doppler measurements of low velocity blood flow: Limitations due to clutter signals from vibrating muscles," *IEEE Trans. Ultrason., Ferroelectr., Freq. Control*, vol. 44, no. 4, pp. 873–881, Jul. 1997.
- [4] D. E. Goertz *et al.*, "High frequency nonlinear B-scan imaging of microbubble contrast agents," *IEEE Trans. Ultrason., Ferroelectr., Freq. Control*, vol. 52, no. 1, pp. 65–79, Jan. 2005.
- [5] C. Errico *et al.*, "Ultrafast ultrasound localization microscopy for deep super-resolution vascular imaging," *Nature*, vol. 527, no. 7579, pp. 499–502, Nov. 2015.
- [6] C. Tremblay-Darveau, R. Williams, L. Milot, M. Bruce, and P. N. Burns, "Combined perfusion and Doppler imaging using plane-wave nonlinear detection and microbubble contrast agents," *IEEE Trans. Ultrason., Ferroelectr., Freq. Control*, vol. 61, no. 12, pp. 1988–2000, Dec. 2014.
- [7] C. Tremblay-Darveau, R. Williams, Z. Zhang, L. Milot, M. Bruce, and P. N. Burns, "Adapting amplitude modulation to plane-wave non-linear Doppler imaging," in *Proc. IEEE Int. Ultrason. Symp. (IUS)*, Sep. 2014, pp. 1742–1745.
- [8] C. Tremblay-Darveau, R. Williams, L. Milot, M. Bruce, and P. N. Burns, "Visualizing the tumor microvasculature with a nonlinear plane-wave Doppler imaging scheme based on amplitude modulation," *IEEE Trans. Med. Imag.*, vol. 35, no. 2, pp. 699–709, Feb. 2016.
- [9] Z. Z. Khaing *et al.*, "Contrast-enhanced ultrasound to visualize hemodynamic changes after rodent spinal cord injury," *J. Neurosurg., Spine*, vol. 29, no. 3, pp. 306–313, Sep. 2018. [Online]. Available: <https://thejns.org/view/journals/j-neurosurg-spine/29/3/article-p306.xml>
- [10] D. H. Simpson, C. Ting Chin, and P. N. Burns, "Pulse inversion Doppler: A new method for detecting nonlinear echoes from microbubble contrast agents," *IEEE Trans. Ultrason., Ferroelectr., Freq. Control*, vol. 46, no. 2, pp. 372–382, Mar. 1999.
- [11] T. Faez, M. Emmer, K. Kooiman, M. Versluis, A. van der Steen, and N. de Jong, "20 years of ultrasound contrast agent modeling," *IEEE Trans. Ultrason., Ferroelectr., Freq. Control*, vol. 60, no. 1, pp. 7–20, Jan. 2013.
- [12] M. Bruce, M. Averkiou, K. Tiemann, S. Lohmaier, J. Powers, and K. Beach, "Vascular flow and perfusion imaging with ultrasound contrast agents," *Ultrasound Med. Biol.*, vol. 30, no. 6, pp. 735–743, Jun. 2004.
- [13] G. Montaldo, M. Tanter, J. Bercoff, N. Benech, and M. Fink, "Coherent plane-wave compounding for very high frame rate ultrasonography and transient elastography," *IEEE Trans. Ultrason., Ferroelectr., Freq. Control*, vol. 56, no. 3, pp. 489–506, Mar. 2009.
- [14] C. Demené *et al.*, "Spatiotemporal clutter filtering of ultrafast ultrasound data highly increases Doppler and fUltrasound sensitivity," *IEEE Trans. Med. Imag.*, vol. 34, no. 11, pp. 2271–2285, Nov. 2015.
- [15] C. Tremblay-Darveau *et al.*, "Improved contrast-enhanced power Doppler using a coherence-based estimator," *IEEE Trans. Med. Imag.*, vol. 36, no. 9, pp. 1901–1911, Sep. 2017.
- [16] C. Kasai, K. Namekawa, A. Koyano, and R. Omoto, "Real-time two-dimensional blood flow imaging using an autocorrelation technique," *IEEE Trans. Sonics Ultrason.*, vol. SU-32, no. 3, pp. 458–464, May 1985.
- [17] T. Xu and G. R. Bashford, "Lateral blood flow velocity estimation based on ultrasound speckle size change with scan velocity," *IEEE Trans. Ultrason., Ferroelectr., Freq. Control*, vol. 57, no. 12, pp. 2695–2703, Dec. 2010.
- [18] C. Sun, V. Sboros, M. B. Butler, and C. M. Moran, "In vitro acoustic characterization of three phospholipid ultrasound contrast agents from 12 to 43 MHz," *Ultrasound Med. Biol.*, vol. 40, no. 3, pp. 541–550, Mar. 2014.
- [19] M. Bruce, C. Tremblay-Darveau, C. Fraschini, and P. Burns, "Ultrafast imaging of microbubbles," in *Proc. Eur. Symp. Ultrasound Contrast Imag.*, Rotterdam, The Netherlands: Erasmus MC Rotterdam, 2013, pp. 452–455.
- [20] J. Bercoff *et al.*, "Ultrafast compound Doppler imaging: Providing full blood flow characterization," *IEEE Trans. Ultrason., Ferroelectr., Freq. Control*, vol. 58, no. 1, pp. 134–147, Jan. 2011.
- [21] J. Baranger, B. Arnal, F. Perren, O. Baud, M. Tanter, and C. Demene, "Adaptive spatiotemporal SVD clutter filtering for ultrafast Doppler imaging using similarity of spatial singular vectors," *IEEE Trans. Med. Imag.*, vol. 37, no. 7, pp. 1574–1586, Jul. 2018.
- [22] H.-C. Han, "Twisted blood vessels: Symptoms, etiology and biomechanical mechanisms," *J. Vascular Res.*, vol. 49, no. 3, pp. 185–197, 2012.
- [23] K. Christensen-Jeffries *et al.*, "Super-resolution ultrasound imaging," *Ultrasound Med. Biol.*, vol. 46, no. 4, pp. 865–891, 2020.
- [24] R. J. G. van Sloun *et al.*, "Super-resolution ultrasound localization microscopy through deep learning," 2018, *arXiv:1804.07661*. [Online]. Available: <http://arxiv.org/abs/1804.07661>
- [25] R. J. G. van Sloun, O. Solomon, M. Bruce, Z. Z. Khaing, Y. C. Eldar, and M. Mischi, "Deep learning for super-resolution vascular ultrasound imaging," in *Proc. IEEE Int. Conf. Acoust., Speech Signal Process. (ICASSP)*, May 2019, pp. 1055–1059.
- [26] A. Bar-Zion, O. Solomon, C. Tremblay-Darveau, D. Adam, and Y. C. Eldar, "SUSHI: Sparsity-based ultrasound super-resolution hemodynamic imaging," *IEEE Trans. Ultrason., Ferroelectr., Freq. Control*, vol. 65, no. 12, pp. 2365–2380, Dec. 2018.



Matthew Bruce received the B.S. and M.S. degrees in electrical engineering from Michigan Technological University, Houghton, MI, USA, in 1992 and 1994, respectively, and the Ph.D. degree in bioengineering from the University of Washington, Seattle, WA, USA, in 2004.

He previously worked for Philips Medical Systems, Bothell, WA, USA, and Supersonic Imagine, Aix-en-Provence, France. He is currently with Center for Industrial and Medical Ultrasound, Applied Physics Laboratory, University of Washington. His interests include ultrasound imaging of blood flow, elastography, and beamformation.



Alex Hannah received the B.S. degree in biomedical engineering from Vanderbilt University, Nashville, TN, USA, in 2009, and the Ph.D. degree from The University of Texas at Austin, Austin, TX, USA, in 2015, studying ultrasound imaging and contrast agents.

He was a Postdoctoral Research Associate with Center for Industrial and Medical Ultrasound, Applied Physics Laboratory, University of Washington, Seattle, WA, USA. He is currently a Systems Engineer with Boston Scientific, Bothell, WA, USA.



Ryan Hammond was born in Tacoma, WA, USA, in 1983. He received the dual B.S. and M.S. degrees in bioengineering from the University of Washington, Seattle, WA, USA, in 2018 and 2020, respectively.

He is currently with Sonosite FujiFilm, Bothell, WA, USA.



Zin Z. Khaing received the B.S. degree in biology from The Catholic University of America, Washington, DC, USA, in 1996, and the M.S. and Ph.D. degrees in cellular, molecular and developmental neuroscience from the Mount Sinai School of Medicine, New York, NY, USA, in 2002 and 2004, respectively.

After her postdoctoral work in the Department of Biomedical Engineering, University of Texas at Austin, Austin, TX, USA, and the University of Florida, Gainesville, FL, USA, she joined the faculty in the Department of Neurological Surgery, University of Washington, Seattle, WA, USA, where she is currently an Assistant Professor. Her research interests are in the areas of central nervous system plasticity after injury and in aging, and spinal cord injury regeneration and repair with expertise in neuroinflammation, neurovasculature, and neural tissue engineering.



Peter N. Burns was born and educated in the United Kingdom, where he took first class honours in theoretical physics. He studied philosophy of science and received the Ph.D. degree in radiodiagnosis from the University of Bristol, Bristol, U.K., in 1974.

He is currently a Professor and the Chair of medical biophysics with the University of Toronto, Toronto, ON, Canada, and a Senior Scientist with Sunnybrook Health Science Centre, Toronto. After his Ph.D., he moved to the United States

in 1984 as an Assistant Professor of radiology at Yale University, New Haven, CT, USA. He then spent four years in the Department of Diagnostic Radiology, Thomas Jefferson University, Philadelphia, PA, USA, before moving to Canada in 1991. His main interest is in blood flow detection and instrumentation for Doppler ultrasound, where he was part of the early efforts to detect blood flow in tumors and other small vessel systems. His current work is with color Doppler instrumentation, hemodynamic measurement with Doppler, and with ultrasound contrast agents.



Charles Tremblay-Darveau was born in Saint-Charles-Borromée, Canada, in 1987. He received the B.Sc. degree in physics from McGill University, Montreal, QC, Canada, in 2009, and the M.S. and Ph.D. degrees in medical biophysics from the University of Toronto, Toronto, ON, Canada, in 2011 and 2015, respectively.

He is currently a System Designer with Philips Healthcare, Bothell, WA, USA. His research interests include nanofluidics, Doppler angiography, contrast-enhanced ultrasound imaging, elastography, and noninvasive blood pressure measurement with microbubbles.



Christoph P. Hofstetter received the M.D. degree from the University of Vienna, Vienna, Austria, in 2005, and the Ph.D. degree from the Karolinska Institute, Stockholm, Sweden, in 2005.

He is currently an Associate Professor with the Department of Neurological Surgery, University of Washington, Seattle, WA, USA. His translational laboratory develops biomarkers for acute spinal cord injury with a focus on novel-ultrasound imaging techniques. It also investigates experimental treatment approaches to mitigate secondary injury following traumatic spinal cord injury. His clinical research interest includes minimally invasive motion preserving spinal procedures with a focus on full-endoscopic techniques.